The Journal of Chemical Physics

Theory meets experiment for unravelling the C1s X-ray photoelectron spectra of pyridine, 2-fluoropyridine, and 2,6-difluoropyridine

Cite as: J. Chem. Phys. **151**, 124105 (2019); https://doi.org/10.1063/1.5122310
Submitted: 31 July 2019 . Accepted: 05 September 2019 . Published Online: 25 September 2019

Marco Mendolicchio, Alberto Baiardi, Giovanna Fronzoni, Mauro Stener, Cesare Grazioli, Monica de Simone, and Vincenzo Barone

The Journal of Chemical Physics ARTICLE scitation.org/journal/jcp

Theory meets experiment for unravelling the C1s X-ray photoelectron spectra of pyridine, 2-fluoropyridine, and 2,6-difluoropyridine

Cite as: J. Chem. Phys. 151, 124105 (2019); doi: 10.1063/1.5122310
Submitted: 31 July 2019 • Accepted: 5 September 2019 •
Published Online: 25 September 2019

Marco Mendolicchio,[1] Alberto Baiardi,[1,2] Giovanna Fronzoni,[3] Mauro Stener,[3] Cesare Grazioli,[4] Monica de Simone,[4] and Vincenzo Barone[1,a)]

AFFILIATIONS

[1]Scuola Normale Superiore, Piazza dei Cavalieri 7, 56125 Pisa, Italy
[2]ETH Zürich, Laboratorium für Physikalische Chemie, Vladimir-Prelog-Weg 2, 8093 Zürich, Switzerland
[3]Dipartimento di Scienze Chimiche e Farmaceutiche, Universita' di Trieste, Via Giorgieri 1, 34127 Trieste, Italy
[4]IOM- CNR Laboratorio TASC, Basovizza SS-14, km 163.5, 34149 Trieste, Italy

[a)]**Author to whom correspondence should be addressed:** vincenzo.barone@sns.it

ABSTRACT

High resolution X-ray photoelectron spectra of a series of substituted pyridines (pyridine, 2-fluoropyridine, and 2,6-difluoropyridine) have been recorded and rationalized by means of a quantum mechanical approach based on the density functional theory including vibronic effects at the Franck-Condon level. The significant chemical shifts of the C1s binding energies induced by fluorine atoms are reproduced quantitatively by our computational model, as well as the vibrational fine structure and the band shapes. Nonsymmetric normal modes play an important role due to the core-hole localization in the presence of equivalent carbon atoms in pyridine and 2,6-difluoropyridine.

I. INTRODUCTION

X-ray Photoelectron Spectroscopy (XPS) is nowadays a widely diffuse technique, mainly employed to study the surfaces of complex materials[1,2] and having consolidated industrial applications.[3] XPS can also be employed to investigate molecules in the gas phase with a high degree of accuracy and information.[4–7] The most direct information that can be extracted from XPS spectra are the Binding Energies (BEs) of the core electrons and their shifts with respect to a reference. Binding energies are the result of the combination of initial and final state effects.[8,9] Initial state effects are determined by the Ground State (GS) before the formation of the core hole and are the consequence of different electron density distributions, for example generated by electronegative substituents, or different coordination numbers. Final state effects are instead mostly related to the relaxation of the electron density upon core hole formation, the most relevant being electron relaxation. Thanks to modern synchrotron light sources, high-resolution XPS spectra can be recorded, from which it is possible to extract additional information based on the fine structure of the absorption bands. Such information is more complicated to be rationalized since it is affected by nuclear motion, decay mechanisms, as well as the cross section of the primary ionization. For all these reasons, a comparison with theoretical models is often necessary to support the interpretation of the experiment. An illustrative example is the ethyl trifluoroacetate (the "ESCA molecule") which has recently been critically reviewed.[10] The theoretical description of the effects of the nuclear motion on XPS spectra can be very demanding. For very small systems, it is possible to calculate the vibro-electronic (vibronic) XPS spectrum beyond the Born-Oppenheimer and Franck-Condon approximations based on Potential Energy Surfaces (PES) and nonadiabatic couplings obtained from correlated electronic-structure calculations.[11] Simplified schemes must, however, be employed for larger molecules in order to reduce the computational efforts while retaining the key physical effects.

In general, the vibrational structure can be important for core electron ionization. In fact, although core orbitals have obviously a nonbonding nature, the dramatic relaxation of the electronic

structure caused by the core hole formation can significantly alter the equilibrium geometry as well as the interatomic forces, introducing relevant vibrational features in the XPS spectra.[12] More specifically, when a geometry change caused by the core-hole formation overlaps with a given normal mode, the corresponding Frank-Condon factor is expected to become large and, concomitantly, relevant in the XPS spectrum. This general effect gives rise to interesting consequences when the molecule contains equivalent atomic sites. In this case, the core hole can localize on one specific atomic site, thanks to the coupling between the electronic and nuclear degrees of freedom, lowering the symmetry of the equilibrium geometry in the presence of the core hole. Therefore, nontotally symmetric normal modes, which one expects to be inactive in the GS geometry, become active due to this symmetry lowering.[13]

In this work, we employ for the description of the nuclear motion a computational scheme previously applied to the simulation of X-Ray absorption spectra of polycyclic aromatic hydrocarbons,[14] which has proven to be quantitatively accurate and efficient to describe the vibrationally resolved Near-Edge X-ray Absorption Fine Structure (NEXAFS) spectra of large molecules. Present XPS calculated spectra are compared with respect to experimental data of state-of-the-art quality, with the two-fold aim of validating the computational scheme and assigning the recorded spectra.

II. COMPUTATIONAL MODEL

All the electronic structure calculations have been performed with methods rooted in the Density Functional Theory (DFT) with the help of the ADF program.[15,16] The B3LYP exchange-correlation functional[17] has been employed in conjunction with Slater Type Orbitals (STO) of Double Zeta plus Polarization (DZP) quality, for all the atoms except the atom carrying the core hole, whose basis set has been improved to all electron Even Tempered Quadruple Zeta plus 3 Polarization (ET-QZ3P) functions. The localization of the core hole is easily realized since only for the atom carrying the core hole an all electron basis set is used, while for the other C atoms, a frozen core basis set is employed. In order to allow localization of the core hole, the symmetry of the system has been properly reduced. Since the nuclear charge is less shielded by the reduced occupation of the 1s orbital carrying the core-hole, the valence orbitals feel an enhanced attraction with respect to the nucleus, and therefore, they become more compact than those in the GS, such an effect being referred to as relaxation. Also for N atoms, a frozen core basis set is employed.

The first step of the theoretical scheme consists in the optimization of the GS geometry, followed by a frequency calculation in order to obtain the GS Hessian matrix as well as the normal modes. In the next step, the localized core-hole ionic configuration at the GS geometry is calculated, in order to obtain the vertical C1s Binding Energy (BE). Such calculation is supplemented by a gradient calculation, which is employed for the following Vertical Gradient (VG) treatment of the nuclear motion.[18] More precisely, the BEs are calculated by means of the ΔKS scheme as energy differences between the core-hole and the GS energies (E_g). A spin polarized unrestricted scheme has been adopted to describe the ionic configuration

$$IP_{1s} = E\left(\left|1s\alpha^1 \ldots\right|\right) - E_g,$$

where $E\left(\left|1s\alpha^1 \ldots\right|\right)$ represents the total energy of a spin-polarized Full Core-Hole (FCH) state.

The information regarding the Hessian of the GS and the gradients calculated with the core hole configuration is extracted from the TAPE21 binary file generated by the ADF program by means of an interface program developed by the authors.

The vibrationally resolved spectra have been computed within the general theoretical framework introduced previously (more details can be found in Refs. 18–22) based on a time-independent (TI) formulation. With this scheme, the intensity of each vibronic excitation is related to the transition dipole moment between the initial and final states of the transition $\left\langle \overline{\overline{\Psi}}\middle|\boldsymbol{\mu}\middle|\overline{\Psi}\right\rangle$, calculated with the following approximations. First of all, the nuclear and electronic degrees of freedom are separated assuming the Born-Oppenheimer approximation and roto-vibrational couplings are minimized by enforcing the Eckart conditions. Under these assumptions, the transition dipole moment can be expressed as $\left\langle \overline{\overline{\chi}}_m\middle|\boldsymbol{\mu}^e_{fi}\middle|\overline{\chi}_n\right\rangle$ where $\overline{\chi}_n$ and $\overline{\overline{\chi}}_m$ are the vibrational levels of the initial and final electronic states involved in the vibronic transition, and $\boldsymbol{\mu}^e_{fi}$ is the electronic transition dipole moment between the initial and final electronic levels, which is in general a function of the nuclear coordinates Q. Assuming the Franck-Condon approximation in the present work, the dependence of the electric transition dipole moment with respect to nuclear coordinates Q is neglected. The harmonic approximation is then used to calculate vibrational levels, neglecting mode-mixing, so the normal modes and frequencies are actually calculated only for the GS and are assumed to be the same for the ionic state as well. The shift vector K (geometry change upon core hole formation) is therefore obtained from ground state frequencies and gradients calculated with the core-hole electron configuration at the GS geometry. This simplified model is usually referred to as the VG and is equivalent to the so-called Linear Coupling Model (LCM).[23] By using all the approximations outlined above, the vibronic spectrum is expressed in terms of the overlap integrals $\left\langle \overline{\overline{\chi}}_m\middle|\overline{\chi}_n\right\rangle$, usually referred to as Franck-Condon integrals.

$\boldsymbol{\mu}^e_{fi}$ corresponds to the dipole integral between the 1s core orbital and the continuum orbital of the unbound photoelectron. In the present experiment, the photon energy employed (382 eV) corresponds to a photoelectron energy above 87 eV, since the binding energies are always below 295 eV. We expect that for this photoelectron energy, $\boldsymbol{\mu}^e_{fi}$ would be in practice identical for all the different core ionizations considered. As a matter of fact, the cross section of core orbitals reaches the atomic limit within at most 10–20 eV above the ionization limit and does not feel the molecular potential any more. For this reason, we set this term arbitrary to unity multiplied by the number of symmetry equivalent sites.

III. EXPERIMENTAL SETUP

The used samples were purchased from Sigma-Aldrich (pyridine, C_5H_5N, 99% purity; 2-fluoropyridine, C_5H_4FN, 98% purity; and 2,6-difluoropyridine, $C_5H_3F_2H$, 99% purity). All samples are liquid at room temperature, so it was possible to introduce their vapor in the experimental chamber through a gas line. To eliminate all traces of air and other possible contaminants, samples were subject to several cycles of freezing and pumping *in situ*. Finally, the temperature was slowly raised and maintained at 295 K.

The C 1s spectra have been recorded at a photon energy of 382 eV and with an overall resolution around 80 meV for pyridine and 2-fluoropyridine. In the case of 2,6-fluoropyridine, its low vapor pressure required us to record the spectrum with a higher photon flux and a resolution of 165 meV. Finally, spectra have been calibrated against the C1s in the CO_2 (297.6 eV) line.

The XPS spectra have been recorded at the GAs-Phase pHotoemission (GAPH) beamline of the Elettra synchrotron, Trieste,[24] and the data were recorded using a VG-Scienta SES-200 photoelectron analyzer[25] which was mounted at a magic angle of 54.7°. The overall resolution was around 80 meV for pyridine and 2-fluoropyridine C1s, while it was not possible to record 2,6-fluoropyridine with a resolution better than 165 meV (see the supplementary material).

IV. RESULTS AND DISCUSSION

Figure 1 shows a comparison between the experimental and simulated spectra for the three molecules under study: the agreement is excellent, with only a slight overall blue-shift of the spectrum (less than 0.2 eV) for 2,6-difluoropyridine.

The XPS spectra of the three molecules are characterized by a complex structure between 291 and 292 eV. Moreover, a separate intense band is present at 293.8 and 284.12 eV for 2-fluoropyridine and 2,6-difluoropyridine, respectively. The shape of all bands, especially those between 291 and 292 eV, is strongly asymmetric due to the presence of significant vibronic effects that are correctly reproduced by the simulations. In order to disentangle the intricate spectral features, in Fig. 2, we report the vibronic calculated spectrum with the individual contribution of each site of the localized core-hole for each molecule. The continuous colored curves are obtained by convoluting all vibronic transitions, while the vertical bars correspond to the vertical BE.

In Table I, we report the vertical BEs and the energies of the most intense vibronic transitions together with their Franck-Condon factors (FC) > 0.10, while Figs. 3–5 provide a graphical representation of the most active modes of each molecules. A more extended table, including transitions with FC < 0.10 has been reported in the supplementary material. Figures S4–S6 of the supplementary material show the details of the vibrational progressions of each *Ci* line. The role of vibrational modulation effects can be judged by comparison of purely electronic and vibronic computed spectra (see Fig. S7).

The C1s theoretical vibronic XPS spectrum of pyridine depicted in Fig. 2 (upper panel) shows that the three-peaked structure around 291 eV in the experimental spectrum is derived from the contribution of the three chemically shifted carbon lines, each with a complex vibrational structure. Based on the ΔKS BEs of the *Ci* core orbitals (reported in Table I), we can attribute the higher energy peak to the C2; its proximity to the electronegative N atom reduces the electrostatic shielding at the C nucleus with a resulting increase of the BE compared to the C3 and C4 atoms. Therefore, the latter atoms contribute to the lower energy side of the spectral structure. The lower BE of C3 with respect to C4 can be explained by polarization effects: the positive polarized C2 site leads to a negative polarized C3 atom and a slightly positive polarized C4 atom, with an alternating behavior typical of substituted benzenes.[26] The computed chemical shifts between the C3 and C4 vertical BEs (300 meV) and the C4 and C2 ones (360 meV) are in excellent agreement

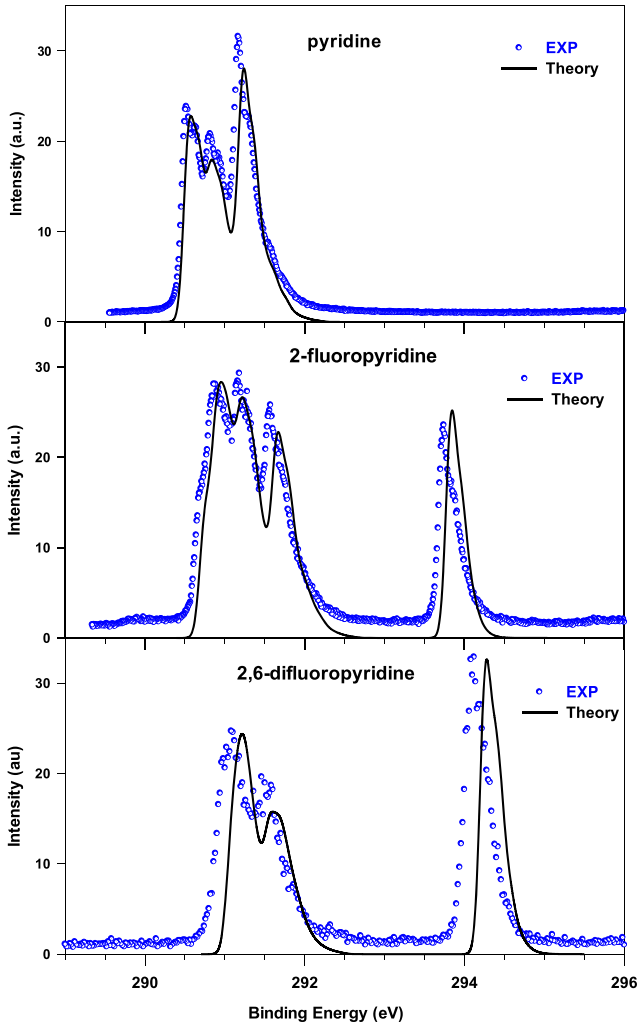

FIG. 1. C1s XPS spectra (circles) of pyridine, 2-fluoropyridine, and 2,6-difluoropyridine. The full lines show the calculated results including vibronic coupling at the VG|FC level. Gaussian distribution functions with a HWHM of 0.07 eV have been used to simulate broadening effects.

with the experimental values of 300 meV and 350 meV, respectively, obtained as the difference between the first fitted experimental energy value of each site. The calculated vibronic spectrum reproduces quantitatively the experimental vibrational energies and their intensity. Figure S4 of the supplementary material clearly shows that the vibrational progression of each *Ci* line is dominated by the vibronic transition between the vibrational ground states of the two electronic states (referred to as 0–0 in the following), suggesting that the change of geometry upon ionization is relatively small. The 0–0 excitation energy computed for C2, C3, and C4 sites is in excellent agreement with the corresponding first fitted experimental energy value, as evidenced by Table I. A limited number of other transitions with lower intensities contribute to the overall band-shape (see Fig. S4 of the supplementary material). The strongest contribution

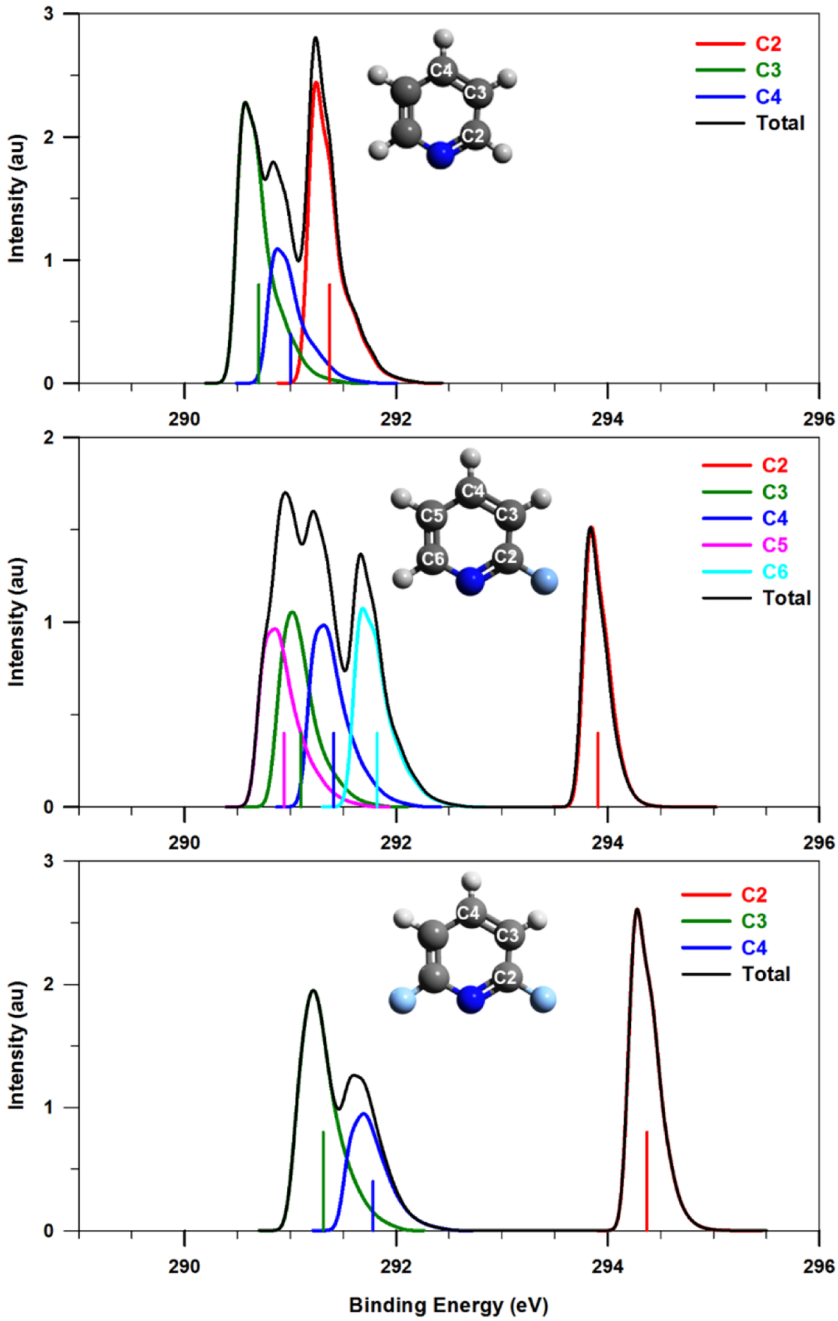

FIG. 2. Vibronic VG|FC C1s XPS spectra (black line) of pyridine (upper panel), 2-fluoropyridine (middle panel), and 2,6-difluoropyridine (lower panel). Colored profiles show the convoluted vibronic spectrum for each nonequivalent Ci site (as labeled in the molecule). Vertical bars represent the BEs calculated at the ΔKS level with the intensity proportional to the number of equivalent Ci atoms. Gaussian distribution functions with a HWHM of 0.05 eV have been used to simulate broadening effects for each vibronic transition.

to the C2 and C3 spectra is derived from normal mode 13, which corresponds to the in-plane C–H bending mode, while the most important vibrational mode in the C4 ionization is mode 12, which contains C4–H stretching and in plane C–H bending involving the remaining C atoms. Other less pronounced transitions in the three C2, C3, and C4 spectra correspond to the in-plane modes (modes 3,4, and 10), which involve also the displacement of the N atom, as shown in Fig. 3.

There are five nonequivalent *Ci* sites in the 2-fluoropyridine molecule; the direct bonds with nitrogen and fluorine decrease the shielding effects for the C2 carbon atom and give rise to the highest energy signal at 293.91 eV. The other four carbon atoms (C3, C4, C5, and C6) contribute to the complex, lower energy feature of the spectrum around 291.5 eV. The spectrum obtained for the ionization of the C6 site gives rise to the peak at a higher BE (291.82 eV), due to polarization effects of the electronegative N atom. Three

TABLE I. Calculated vertical BEs, vibrational excitations, and Franck-Condon factors and related normal modes of pyridine, 2-fluoropyridine, and 2,6-difluoropyridine for each nonequivalent carbon site. Experimental energies are included for comparison. The numbers in brackets represent the margin of error on the last digit.

Carbon site	Vertical BE (eV)	Vibronic excitation energy (eV)	Franck-Condon factor[a]	Assignment	Experiment[b]
		Pyridine			
C3	290.70	290.53	0.7415	0	290.51(1)
		290.62	0.1056	4^1	290.64(1)
		290.66	0.1772	10^1	290.75(6)
		290.67	0.2368	13^1	
C4	291.00	290.83	0.3258	0	290.81(1)
		290.91	0.0832	3^1	290.93(1)
		290.96	0.1158	12^1	291.04(1)
C2	291.37	291.20	0.8430	0	291.17(1)
		291.34	0.0850	10^1	291.31(1)
		291.35	0.2273	13^1	291.44(1)
					291.58(1)
					291.74(1)
		2-fluoropyridine			
C5	290.94	290.73	0.2333	0	290.69(1)
		290.86	0.1084	14^1	290.85(2)
					290.99(2)
C3	291.10	290.89	0.1506	0	291.15(1)
		290.95	0.1140	3^1	
C4	291.41	291.21	0.2614	0	291.31(3)
		291.34	0.1149	14^1	
C6	291.82	291.65	0.3224	0	291.56(1)
					291.71(2)
C2	293.91	293.83	0.4848	0	293.74(1)
					293.90(1)
		2,6-difluoropyridine			
C3	291.31	291.06	0.1966	0	291.07(1)
C4	291.78	291.56	0.2025	0	291.48(2)
		291.65	0.1175	10^1	291.78(6)
		291.69	0.1157	16^1	292.24(5)
C2	294.37	294.25	0.7415	0	294.10(1)
		294.32	0.1830	6^1	294.32(2)
		294.40	0.1587	18^1	

[a]Only Franck-Condon factors larger than 10% of the total sum for each *Ci* are listed together with all transitions with experimental counterparts.
[b]See the supplementary material for the experimental fitting procedure.

chemically shifted carbon lines contribute to the two-peaked profile around 291 eV. The BEs of C5 and C3 sites (290.94 and 291.10 eV) are shifted to lower energy compared to C4 (291.41 eV) due to the negative polarization induced by the C6 and C2 atoms, respectively.

The comparison of the ΔKS BEs of the *Ci* sites contributing to the lower energy feature with the first experimental energy reported in Table I reveals a general good agreement between theory and experiment, with a major discrepancy found for the C5 BE, which is overestimated by the theory by about 250 meV. A

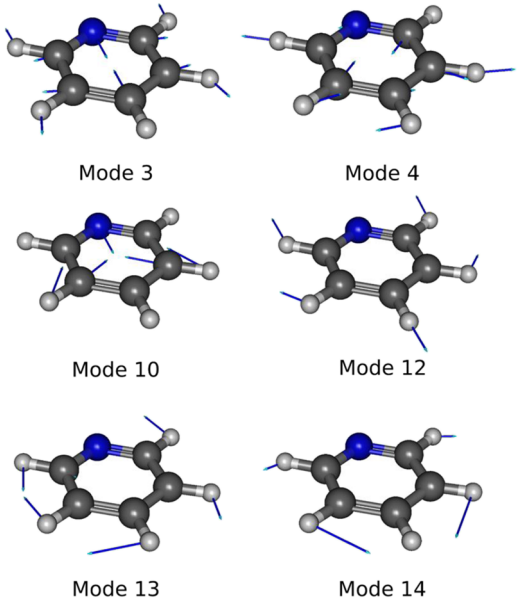

FIG. 3. Graphical representation of the normal modes of pyridine giving the most intense vibronic transitions in the C1s XPS spectrum.

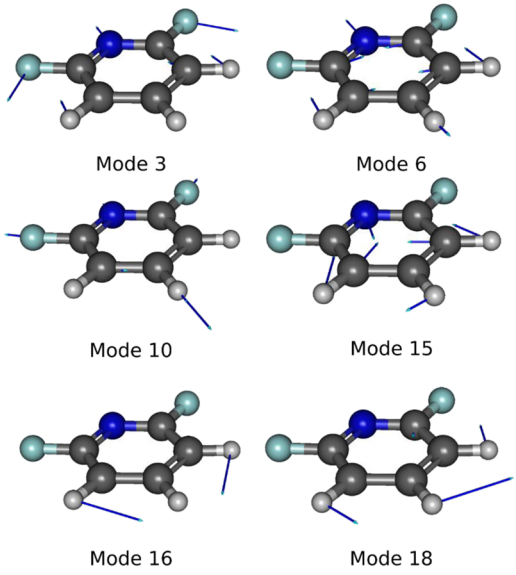

FIG. 5. Graphical representation of the normal modes of 2,6-difluoropyridine giving the most intense vibronic transitions in the C1s XPS spectrum.

similar difference with the experiment is found also for the C6 BE. Nevertheless, these discrepancies are well within the accuracy of the computational protocol and the vibronic energies as well as the overall band shape correctly reproduce the experimental data.

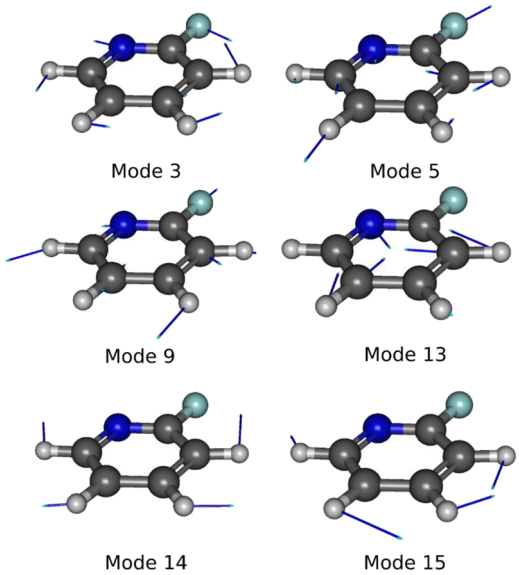

FIG. 4. Graphical representation of the normal modes of 2-fluoropyridine giving the most intense vibronic transitions in the C1s XPS spectrum.

Table I highlights that the 0–0 transition dominates the spectrum of each *Ci* ionization, although its intensity is lower than that found for the pyridine molecule, and that the 0–0 calculated excitation energies are in very good agreement with the experimental energy values, with a maximum deviation of 260 meV in the case of C3 and C6 ionizations. The vibronic profiles of the C2 and C6 sites, bound to the N atom, have different shapes with respect to those of C5, C3, and C4 sites. The latter are in fact characterized by a wide vibrational decay contributed by several quite intense transitions, as shown by Fig. S5 of the supplementary material. The most intense one in the C4 and C5 spectra is attributed to the high energy normal mode 14 (at 291.34 eV) which corresponds to a CCH bending, while the very rich C3 vibrational spectrum is mostly contributed by the lower energy mode 3, associated with in plane CCH and CCF bending, and by mode 9, corresponding to an in plane deformation of the ring (see Fig. 4). The vibronic profiles of the C6 and C2 ionizations are instead rather sharp, in particular, in the case of the C2 site, whose vibronic progression decays in a small energy range. The 0–0 transition of the C2 spectrum has the highest intensity with respect to all the other Ci spectra, in analogy with the behavior found in the pyridine *Ci* spectra. Low-intensity vibrational transitions contribute to the C2 and C6 profiles, the most relevant deriving from in plane deformation modes (5, 9, and 13).

The C1s spectrum of 2,6-difluoropyridine presents two intense bands well separated in energy, in analogy with the 2-fluoropyridine spectrum. The presence of only three nonequivalent *Ci* sites simplifies the lower energy band compared to the corresponding one in the 2-fluoropyridine. The higher energy vibrational peak can be assigned to the C2 atom directly bonded to the F atom, which is strongly deshielded with respect to the C3 and C4 atoms. These latter C atoms contribute to the lower energy, double-peaked vibrational structure. Polarization effects influence the trend of C3 and C4 BEs,

with the C3 site more shielded than the C4 site, as already discussed previously for pyridine. Their calculated chemical shift (470 meV) is in good agreement with the experimental one (410 meV), as well as the C4–C2 chemical shift (2.59 eV and 2.53 eV from theory and experiment, respectively). Due to the presence of the second fluorine atom, the C2 BE is shifted at a higher energy compared to that of the C2 site in the 2-fluoropyridine spectrum. A slight overestimation of the calculated C2 BE makes the agreement with the experiment less quantitative than that for the other two molecules, even if the theory reproduces the shape and relative intensities of all the bands correctly, as shown in Fig. 1. In analogy with the previous cases, the most intense vibronic band of each *Ci* ionization is the 0–0 transition, whose calculated energy agrees well with the first fitted experimental value. The 0–0 transition is particularly intense for the C2 spectrum with respect to C3 and C4 even more markedly than in the previous molecules. The vibrational profiles of the *Ci* sites resemble those observed in 2-fluoropyridine, with the C3 and C4 vibrational decays extended over a larger energy range than the C2 profile (see Fig. S6 of the supplementary material), as observed for the 2-fluoropyridine. The C3 and C4 vibrational profiles are very rich in transitions with a non-negligible intensity mostly associated with in plane CCF and CCH bending modes, as shown in Fig. 5. In addition, several combination bands contribute to the tail at a higher energy giving a broader shape to the spectra. In plane CCH bending modes mainly determine also the C2 vibrational spectrum.

It is worth noting that for both pyridine and 2,6-difluoropyridine, some of the active normal modes are non-totally symmetric, for example, modes 4 and 13 for pyridine (see Fig. 3) and modes 15 and 18 for 2,6-difluoropyridine (see Fig. 5). The presence of such non-totally symmetric normal modes is related to the localization of the core hole on one of the chemically equivalent carbon atoms (C2–C6 or C3–C5), which lowers the symmetry of the ionized state compared to the one of the neutral state. Therefore, also nonsymmetric normal modes, pointing to a broken-symmetry equilibrium geometry for the ion, may be active. Such an effect, as well as the geometry relaxation and symmetry reduction, was analyzed in detail[27] upon core hole formation in excited (NEXAFS) and ionized (XPS) configurations in CO_2, C_2H_4, and C_6H_6. In the present work, we assume the core hole localization, an effect, which has proven to happen in the NEXAFS experiment for C_2H_4.[28] In XPS, the experimental detection of localization of the core hole, with concomitant symmetry breaking, has been inferred from the asymmetry of the angular distribution of the photoelectron in coincidence experiments.[29] As discussed in Ref. 12, a full theoretical characterization of the core-hole localization requires the description of the PESs with a diabatic picture.

The absence of out-of-plane active normal modes for all the molecules considered in the present work demonstrates that the core hole ion maintains the GS planar geometry, excluding pyramidalization effects, in line with previous analysis on C_6H_6.[27]

V. CONCLUSIONS

We presented high resolution C1s XPS gas phase spectra for pyridine, 2-fluoropyridine, and 2,6-difluoropyridine. The experimental spectra were assigned with the help of a new computational DFT scheme for the description of the XPS vibronic fine structure. The method is able to provide a quantitative reproduction of the experimental data, with deviation below 0.2 eV for the vertical BE, and also appears suitable for application to larger systems with reasonable computational effort. The localization of the core hole facilitates the interpretation of the C1s XPS spectra in terms of vibrational excitations associated with each nonequivalent carbon atomic site.

The inclusion of the fluorine atom decreases the shielding effects for the C atom directly bonded to it (C2 site) with a consequent shift of the C2 BE towards higher energy and the appearance of a well separated vibrational feature in the XPS spectra of 2-fluoropyridine and 2,6-difluoropiridine.

The vibrational structures present in the XPS spectra have been analyzed in terms of normal modes involved in the vibrational spectrum of each *Ci* nonequivalent site. The vibronic profiles are always dominated by the 0–0 transitions and the main vibrations are associated with in plane CCH and CCF bending modes. The C2 0–0 transition is more intense with respect to that of the other Ci sites of each molecule and this difference increases on going from pyridine to 2,6 difluoropiridine.

The present work confirms the importance of vibrational modulation effects for a direct vis-à-vis comparison of experimental and simulated spectra.

SUPPLEMENTARY MATERIAL

See the supplementary material for a full list of vertical BEs (Table S1); fits of experimental spectra (Figs. S1–S3); VG|FC vibronic stick spectra (Figs. S4–S6); and comparison between vibronic and vertical electronic spectra (Fig. S7).

ACKNOWLEDGMENTS

We thank Dr. Marcello Coreno and Dr. Antti Kivimaki for helpful suggestions as well as for their help during the set-up of the high resolution XPS measurements and C. Puglia (Uppsala University, Sweden) and the Carl Trygger Foundation for making available the VG-Scienta SES-200 photoelectron analyzer at the gas phase beamline, Elettra, Italy.

Computational research was supported by Stiftung Beneficentia and by Finanziamento per ricerca di ateneo, Grant Nos. FRA 2015 and FRA 2016 of the Università degli Studi di Trieste.

REFERENCES

[1] J. F. Watts, *An Introduction to Surface Analysis by XPS and AES* (J. Wiley, New York, 2003).
[2] P. Van der Heide, *X-ray Photoelectron Spectroscopy An Introduction to Principles and Practices* (Wiley-Blackwell. Hoboken, NJ, 2012).
[3] J. Electron Spectrosc. Relat. Phenom. **231**, 1–140 (2019), special issue on "Applications of XPS in Industry," edited by S. R. Bare, S. Thevuthasan, and C. Richard Brundle.
[4] C. Nordling, E. Sokolowski, and K. Siegbahn, Ark. Fys. **12**, 301 (1957).
[5] C. Nordling, E. Sokolowski, and K. Siegbahn, Phys. Rev. **105**, 1676 (1957).
[6] K. Siegbahn, C. Nordling, A. Fahlman, R. Nordberg, K. Hamrin, J. Hedman, G. Johansson, T. Bergmark, S.-E. Karlsson, I. Lindgren, and B. Lindberg, *ESCA, Atomic, Molecular and Solid State Structure Studied by Means of Electron Spectroscopy* (Almqvist and Wiksells, Uppsala, 1967).
[7] K. Siegbahn, K. Nordling, G. Johansson, J. Hedman, P. Hedén, K. Hamrin, U. Gelius, L. W. T. Bergmark, R. Manne, and Y. Baer, *ESCA Applied to Free Molecules* (North-Holland, Amsterdam, London, 1969).

[8]P. Bagus, C. Sousa, and F. Illas, Theor. Chem. Acc. **138**, 61 (1993).
[9]P. Bagus, G. Pacchioni, and F. Parmigiani, Chem. Phys. Lett. **207**, 569 (1993).
[10]O. Travnikova, K. J. Børve, M. Patanen, J. Söderström, C. Miron, L. J. Sæthre, N. Mårtensson, and S. Svensson, J. Electron Spectrosc. Relat. Phenom. **185**, 191 (2012).
[11]N. V. Dobrodey, H. Köppel, and L. S. Cederbaum, Phys. Rev. A **60**, 1988 (1999).
[12]V. Myrseth, K. J. Børve, K. Wiesner, M. Bässler, S. Svensson, and L. J. Sæthre, Phys. Chem. Chem. Phys. **4**, 5937 (2002).
[13]I. Minkov, F. Gel'mukhanov, R. Friedlein, W. Osikowicz, C. Suess, G. Öhrwall, S. L. Sorensen, S. Braun, R. Murdey, W. R. Salaneck, and H. Ågren, J. Chem. Phys. **121**, 5733 (2004).
[14]A. Baiardi, M. Mendolicchio, V. Barone, G. Fronzoni, G. A. Cardenas Jimenez, M. Stener, C. Grazioli, M. de Simone, and M. Coreno, J. Chem. Phys. **143**, 204102 (2016).
[15]E. J. Baerends, D. E. Ellis, and P. Ros, Chem. Phys. **2**, 41 (1973).
[16]C. Fonseca Guerra, J. G. Snijders, G. te Velde, and E. T. Baerends, Theor. Chem. Acc. **99**, 391 (1998).
[17]C. Lee, W. Yang, and R. G. Parr, Phys. Rev. B **37**, 785 (1988).
[18]C. Puzzarini, J. Bloino, N. Tasinato, and V. Barone, Chem. Rev. **119**, 8131 (2019).
[19]A. Baiardi, J. Bloino, and V. Barone, J. Chem. Theory Comput. **9**, 4097 (2013).
[20]V. Barone, Wiley Interdiscip. Rev.: Comput. Mol. Sci. **6**, 86 (2016).
[21]A. Baiardi, L. Paoloni, V. Barone, V. G. Zakrzewski, and J. V. Ortiz, J. Chem. Theory Comput. **13**, 3120 (2017).
[22]V. Barone, A. Baiardi, M. Biczysko, J. Bloino, C. Cappelli, and F. Lipparini, Phys. Chem. Chem. Phys. **14**, 12404 (2012).
[23]P. Macak, Y. Luo, and H. Ågren, Chem. Phys. Lett. **330**, 447 (2000).
[24]R. Blyth, R. Delaunay, M. Zitnik, J. Krempasky, R. Krempaska, J. Slezak, K. Prince, R. Richter, M. Vondracek, R. Camilloni, L. Avaldi, M. Coreno, G. Stefani, C. Furlani, M. de Simone, S. Stranges, and M.-Y. Adam, "The high resolution gas phase photoemission beamline, Elettra," J. Electron Spectrosc. Relat. Phenom. **101-103**, 959–964 (1999).
[25]A. Kivimaki, P. Norman, M. Coreno, M. de Simone, C. Grazioli, R. Totani, B. Ressel, H. Ottosson, and C. Puglia, Phys. Rev. A **88**, 062502 (2013).
[26]C. Kolczewski, R. Püttner, O. Plashkevych, H. Ågren, V. Staemmler, M. Martins, G. Snell, A. S. Schlachter, M. Sant'Anna, G. Kaindl, and L. G. M. Pettersson, J. Chem. Phys. **115**, 6426 (2001).
[27]P. Norman and H. Ågren, J. Mol. Struct.: THEOCHEM **401**, 107 (1997).
[28]F. X. Gadea, H. Köppel, J. Schirmer, L. S. Cederbaurn, K. J. Randall, A. M. Bradshaw, Y. Ma, F. Sette, and C. T. Chen, Phys. Rev. Lett. **66**, 883 (1991).
[29]R. Guillemin, P. Decleva, M. Stener, C. Bomme, T. Marin, L. Journel, T. Marchenko, R. H. K. Kushawaha, K. Jänkälä, N. Trcera, K. P. Bowen, D. W. Lindle, M. N. Piancastelli, and M. Simon, Nat. Commun. **6**, 6166 (2015).